



**QUEEN'S  
UNIVERSITY  
BELFAST**

## Evaluation of the anisotropic mechanical properties of reinforced polyurethane foams

Hamilton, A. R., Thomsen, O. T., Madaleno, L. A. O., Rosgaard Jensen, L., Rauhe, J. C. M., & Pyrz, R. (2013). Evaluation of the anisotropic mechanical properties of reinforced polyurethane foams. *Composites Science and Technology*, 87, 210-217. <https://doi.org/10.1016/j.compscitech.2013.08.013>

**Published in:**  
Composites Science and Technology

**Document Version:**  
Peer reviewed version

**Queen's University Belfast - Research Portal:**  
[Link to publication record in Queen's University Belfast Research Portal](#)

### **Publisher rights**

© 2015, Elsevier. Licensed under the Creative Commons Attribution -NonCommercial-NoDerivs License (<https://creativecommons.org/licenses/by-nc-nd/4.0/>), which permits distribution and reproduction for non-commercial purposes, provided the author and source are cited.

### **General rights**

Copyright for the publications made accessible via the Queen's University Belfast Research Portal is retained by the author(s) and / or other copyright owners and it is a condition of accessing these publications that users recognise and abide by the legal requirements associated with these rights.

### **Take down policy**

The Research Portal is Queen's institutional repository that provides access to Queen's research output. Every effort has been made to ensure that content in the Research Portal does not infringe any person's rights, or applicable UK laws. If you discover content in the Research Portal that you believe breaches copyright or violates any law, please contact [openaccess@qub.ac.uk](mailto:openaccess@qub.ac.uk).

# Evaluation of the Anisotropic Mechanical Properties of Reinforced Polyurethane Foams

Andrew R. Hamilton<sup>a,1\*</sup>, Ole Thybo Thomsen<sup>b,a</sup>, Liliana A. O. Madaleno<sup>a</sup>, Lars Rosgaard Jensen<sup>a</sup>, Jens Christian M. Rauhe<sup>a</sup>, Ryszard Pyrz<sup>a</sup>

<sup>a</sup>Department of Mechanical and Manufacturing Engineering, Aalborg University, Fibigerstræde 16, 9200 Aalborg East, Denmark

<sup>b</sup>Faculty of Engineering and the Environment, University of Southampton, Highfield, Southampton, SO17 1BJ, UK

\* Corresponding author e-mail address: a.hamilton@qub.ac.uk

Telephone: +44 (0)28 9097 4116

Keywords: A. Particle-reinforced composites, A. Nano composites, B. Porosity/Voids, C. Elastic properties, Cellular materials

## Abstract

The mechanical impact of adding milled glass fibers and nanoparticles at different mass fractions to low-density (relative density  $< 0.2$ ) polyurethane (PU) foams is investigated. Tensile, compressive, and shear stress-strain curves are measured in the plane parallel to the foam-rise direction and the in-plane components of the elastic modulus are determined in order to assess the mechanical anisotropy of the foams. Power-law relationships between the moduli and apparent density are established for pure PU foams and used as a baseline to which the properties of composite foams are compared. Cellular mechanics models based on both rectangular and Kelvin unit-cell geometries are employed to estimate changes in the cell shape based on the mechanical anisotropy of composite foams, and the model results are compared with direct observations of the cellular structure from microscopy. A single measure of foam stiffness reinforcement is defined that excludes the effects of the apparent foam density and cell shape. The analysis reveals the large impact of cell shape on the moduli of the glass-fiber and nanocomposite foams. Nanocomposite foams exhibit up to an 11.1% degree of reinforcement, and glass-fiber foams up to 18.7% using this method for quantifying foam reinforcement, whereas a simple normalization to the in-plane modulus components of the pure PU foam would

---

<sup>1</sup> Present address: School of Mechanical and Aerospace Engineering, Queen's University Belfast, Ashby Building, Stranmillis Road, Belfast BT9 5AH, Northern Ireland.

indicate from -40.5% to 25.9% reinforcement in nanocomposite foams, and -7.5 to 20.2% in glass-fiber foams.

## **1. Introduction**

Cellular materials are widely used in the energy and transport industries as lightweight structural materials, most notably as the core material in structurally-efficient sandwich panels. Even in nonstructural applications, like packaging or insulation, the mechanical performance and integrity of these materials can be critical. Reinforcing polymer foams with short-fiber or particulate additives is a potential route to improve the mechanical properties, and reduce the weight and cost of these materials. Polyurethane (PU) foams are excellent candidates for targeting mechanical improvement via reinforcement because the mechanical properties of PU foams are relatively poor, and yet the cost and availability compare favorably with alternative foams and natural products (e.g. polyvinylchloride foams and balsa wood).

The mechanical properties of cellular materials are highly dependent upon the cellular structure of the foam, as well as the properties of the solid material making up the foam, both of which may be influenced by reinforcing additives. One of the most important features of the cellular structure in terms of mechanical properties is the void fraction, which is typically characterized by the relative density ( $\rho_f/\rho_s$ ) – defined as the ratio of the density of the foam to that of the bulk material of which the foam is constituted. In foams with a low relative density ( $\rho_f/\rho_s < 0.4$ ), many of the mechanical properties can be related to the relative density according to a power law of the form [1]:

$$\frac{P_f}{P_s} = C \left( \frac{\rho_f}{\rho_s} \right)^n \quad (1)$$

where  $P$  is the mechanical property of interest,  $\rho$  is density, the parameters  $C$  and  $n$  depend on the property of interest and the particulars of the foam (including the foam microstructure and

deformation mode) [2,3,4], and the subscripts s and f indicate the properties of the fully dense solid and of the foam, respectively.

The exponent,  $n$ , in Equation (1) typically ranges from  $1 < n < 2$  for the elastic moduli. A value of  $n = 2$  corresponds to a bending-dominated deformation mode, which is typical of open-cell foams with no cell walls. A value of  $n = 1$  corresponds to stretch-dominated deformation, as might occur in a lattice with members oriented in the direction of loading. Intermediate values of  $n$  are typical in closed-cell foams, which have cell walls that undergo stretching and struts that undergo bending.

Another important attribute for the mechanical properties of cellular materials is the cell shape. In both synthetic and natural cellular materials it is typical for the cell shape to be elongated, leading to anisotropic material properties [1]. The cells of polymer foams tend to be elongated in the direction of foaming (also referred to as the foam rise direction), as shown in Figure 1(a). Mechanical models based on an elongated unit cell have been developed to capture this anisotropic behavior. Huber & Gibson [5] considered a rectangular unit cell (Figure 1(b)) with a cell shape anisotropy ratio,  $R$ , defined as:

$$R = \frac{h}{l}, \quad (2)$$

where  $h$  and  $l$  are the dimensions of the unit cell parallel and perpendicular to the direction of elongation, respectively, as shown in Figure 1(a). This rectangular-cell model predicts transversely isotropic material properties that may be calculated using Equation (1) with an additional term that is related to the shape anisotropy:

$$\frac{P_f}{P_s} = C \left( \frac{\rho_f}{\rho_s} \right)^n f(R) \quad (3)$$

where  $f(R)$  is one of several functions of the shape anisotropy ratio of the unit cell, which are tabulated for the moduli in different material directions in Table 1. According to this model, the



mechanical properties increase in the direction of foaming ( $I$ ) and decrease in all other directions as the shape anisotropy,  $R$ , increases. Using Equation (3), the cell shape anisotropy may be calculated by taking the ratio of the foam moduli in different directions, for example:

$$\frac{E_1}{E_2} = \frac{E_1}{E_3} = \frac{2R^2}{1 + (1/R)^3}, \quad (4)$$

where  $E_1$ ,  $E_2$ , and  $E_3$  are the foam moduli in the material directions defined in Figure 1(a).

The tetrakaidecahedron introduced by Kelvin [6], shown in Figure 1(c), is an alternative cell geometry that is a closer representation of the cellular structure observed in polymer foams than the rectangular cell of Huber & Gibson. In addition to the term  $R$ , the Kelvin cell requires a second term,  $Q$ , to uniquely define the geometry [7]. The impact of varying the parameter  $Q$  on the cell geometry is illustrated in Figure 1(c). The full set of equations for the transversely isotropic material properties as functions of  $P_s$ ,  $\rho_f$ ,  $\rho_s$ ,  $R$ , and  $Q$  are published elsewhere [7,8]. The equivalent expression to Equation (4) using this alternative cellular geometry is:

$$\frac{E_1}{E_2} = \frac{E_1}{E_3} = \frac{R}{4} \left[ \frac{\left( 2\tilde{Q}^2 R^2 + \frac{64Q^3}{\sqrt{16 + \tilde{Q}^2 R^2}} \right) C_1 + \left( 4Q + 2\sqrt{16 + \tilde{Q}^2 R^2} \right) (16 + \tilde{Q}^2 R^2) \left( \frac{\rho_f}{\rho_s} \right)}{16(\sqrt{3} - \pi/2) + \frac{8R^3 \tilde{Q}^5 \left( \frac{20\sqrt{3} - 11\pi}{2\sqrt{3} - \pi} \right)}{(4Q + 2\sqrt{16 + \tilde{Q}^2 R^2}) (16 + \tilde{Q}^2 R^2) \left( \frac{\rho_f}{\rho_s} \right)} \right], \quad (5)$$

where  $\tilde{Q} = 2 + \sqrt{2}Q$ ,  $C_1 = \sqrt{3} - \pi/2$ , and  $C_2 = \frac{20\sqrt{3} - 11\pi}{2\sqrt{3} - \pi}$  for a hypocycloid cross-section [7]. Whereas the properties of the solid do not appear in Equation (4), the relative density is included in Equation (5).

Numerous studies have reported improvements in the mechanical properties of polymer foams reinforced with short fibers [9,10,11,12,13], particles [14,15,16,17,18], and nano-particles [19,20,21,22], but relatively few have made use of cellular models to interpret the results of

mechanical tests and to develop predictive tools. Barma et al. [15] related the foam stiffness ( $E_f$ ) to the solid stiffness ( $E_s$ ) and cell size in particle-reinforced foams at the same density. Saint-Michel et al. [16] modeled reinforced foams with higher relative densities ( $\rho_f/\rho_s > 0.3$ ) as a porous composite filled with closed, isolated, spherical voids. Zhang et al. [20] used a Mori-Tanaka model to account for carbon nanotube reinforcement and cellular voids [23]. Goods et al. [14] used a cellular model in the form of Equation (1) to describe the foam modulus ( $E_f$ ) of PU foams reinforced with metal particles, along with the Kerner equation to account for changes in the solid modulus ( $E_s$ ); others have taken a similar approach with various composite models to estimate  $E_s$  for different materials [13,17,21,22]. The effect of additives on mechanical anisotropy has been reported in several studies on chopped aramid and glass fibers [10,11,12], but was only qualitatively attributed to a combination of cell shape ( $R$ ) and preferential fiber-alignment. Sorrentino et al. [18] reported mechanical anisotropy in foams reinforced with iron particles aligned in a magnetic field, which the authors attributed wholly to the reinforcement and not to cell shape. Nano-scale fillers are known to influence the foaming process by inducing bubble nucleation [19] and have been reported to affect the cell shape [24], yet despite the potential influence of nanoparticles on cellular structure, mechanical anisotropy is often overlooked in the analysis of reinforcement in nanocomposite foams.

A complete picture of the effect of reinforcement on the mechanical properties of composite foams requires mechanical characterization in multiple material directions, and the consideration of these factors related to cellular structure that may be affected by reinforcing additives. In this paper, low-density polyurethane foams ( $\rho_f/\rho_s < 0.2$ ) are characterized in tension and compression in two principal material directions and in shear using a modified Arcan testing fixture [25]. Power-law relationships between the in-plane moduli and density are established for pure PU foams to compensate for density effects in the comparison between composite and pure PU foams. The modulus data are used in conjunction with cellular material models to make

predictions about the cellular structure of the foams that are compared with microscopic observations. Changes in the moduli of composite foams are attributed to changes in the cellular structure (relative density, and cell shape) and to changes in the solid properties ( $\rho_s$ ,  $E_s$ ), and a definition for the degree of foam reinforcement is proposed that is independent of cellular structure and that takes into account the tradeoff between stiffness and density in the mechanical performance of foams.

## **2. Materials and methods**

### *2.1 Foam Preparation*

Rigid, closed-cell PU foams and the precursor components for producing these foams (methylene diphenyl diisocyanate and polyol blends) were obtained from the industrial producer, Recticel<sup>2</sup>. Pure PU foams (with no particle reinforcement) were obtained from the manufacturer in a range of densities ( $\rho_f = 128.0, 153.8, 163.4 \text{ kg-m}^{-3}$ ), and were also produced in the lab under the same conditions as composite foams ( $\rho_f = 144.5 \text{ kg-m}^{-3}$ ).

Montmorillonite–carbon nanotube hybrid nanoparticles were produced by chemical vapour deposition (CVD) onto iron modified montmorillonite [26]. The pre-exfoliated morphology of these hybrid nanoparticles has been observed to result in good dispersion within polymer matrices [27]. Nanocomposite PU foams were prepared by incorporating these hybrid nanoclay/carbon-nanotube particles into the polyol blend before the foaming process, which resulted in better dispersion than incorporation into the diisocyanate, . Prior to use, the hybrid nanoparticles were dried at 110 °C for 24 h in order to remove any water. The hybrid particles were dispersed in the polyol blend at 0.25, 0.5, and 1.0 wt% using a lab homogenizer operating at 3500 rpm for 150 min in an ice bath. The mixture of hybrids dispersed in the polyol was added to the diisocyanate and stirred at 3000 rpm for 25 s. The resulting mixture was quickly poured into a mold and allowed to foam freely in one direction. The resulting foam was cured for 24 h at

---

<sup>2</sup> Recticel N.V. - IDC Corporate, Damstraat 2, B-9230 Wetteren, Belgium.

room temperature and atmospheric pressure. The average density of these nanocomposite foams ranged from 105.3–112.1 kg-m<sup>-3</sup>. The tendency for nanocomposite foams to have lower densities as compared with the lab-produced pure foams has been reported previously [4] and may be explained by the high surface area of the nano-filler and the effects this can have on bubble nucleation and growth during foaming [19].

Milled glass fibers with an average size of 230 microns were obtained from R&G Faserverbundwerkstoffe GmbH<sup>3</sup>. Glass-fiber composite foams were produced with 1.0, 3.0, 5.0, 7.0, 9.0, 11.0, 13.0, 15.0, 17.0, and 19.0 wt% glass fibers. Because the volume of polyol was insufficient to accommodate these high loadings of reinforcement, the glass fibers were dispersed into the diisocyanate using a lab homogenizer operating at 1450 rpm for 5 min. The polyol was premixed at 2850 rpm for 25 s using the homogenizer. The glass-fiber–diisocyanate mixture was cooled to room temperature and added to the premixed polyol and stirred at 2850 rpm for 25 s. The resulting mixture was quickly poured into a mold and allowed to foam freely in one direction. The resulting foam was cured for 24 h at room temperature and atmospheric pressure. The average density of the resulting glass-fiber foams ranged from 131.7–207.5 kg-m<sup>-3</sup>. The tendency for glass-fiber foams to have higher densities as compared with the lab-produced pure foams can be attributed to the higher initial density of the glass-fiber–diisocyanate mixture (especially at the higher filler fractions), which could be expected to hinder foam cell growth.

## 2.2 Mechanical Testing

Mechanical tests were conducted using a modified Arcan fixture (MAF) [25], which allows the application of tensile, compressive, shear, biaxial tensile-shear, or biaxial compressive-shear loads through the spiral configuration of loading holes shown in Figure 2(a). The non-standard

---

<sup>3</sup> R&G Faserverbundwerkstoffe GmbH, Postfach 1145, D-71107 Waldenbuch, Germany.

compact specimen geometries shown in Figure 2(b) were adopted from Taher et al. [25], and were produced using a CNC router. Shear specimens were manufactured with the foam rise direction in the plane of the applied shear (*I*-2 plane). Tension and compression specimens were either oriented with the axis of loading oriented parallel (*I*-direction, designated ‘rise’) or perpendicular (2- and 3-directions, designated ‘transverse’) to the foam rise direction.

Testing was performed at a displacement rate of 0.6 mm/min. on a screw-driven load frame with a 2 kN load transducer to record force data. The state of strain on the front and back surfaces of the specimen was measured by digital image correlation (DIC) [28,29], which was performed using an Aramis metrology system (GOM mbH). Digital images had a typical resolution of 10  $\mu\text{m}/\text{pixel}$  and were acquired at regular intervals throughout testing. Image correlation was performed using a window/facet size of 60 x 60 pixels and a step size of 30 pixels. These parameters were selected because, at >1.5 times the average cell size of the foams being tested, the window size was sufficiently large to yield a relatively homogeneous strain field (strain variation on the size scale of individual foam cells was not of interest in this study). Repeated analyses with window sizes ranging from 10-80 pixels square yielded no significant differences in the resulting stress-strain curves. Representative full-field strain measurements are shown in Figure 3 for each specimen type while loaded in the elastic range.

Stress-strain curves were constructed by averaging the strain data within the gauge area or along the gauge line on both the front and back surfaces of each specimen type (indicated in Figure 2(b)), and computing the nominal stress from the load data associated with each image. The strain data were corrected both for non-uniformity within the gauge zone and for surface effects using models of each specimen type in the commercial finite element (FE) code Abaqus 6.10-2. The results of this FE analysis for the shear specimen indicate a small variation in the shear strain along the gauge line (approx. 5%, as shown in Figure 4(a)), and a larger variation on the

gauge plane through the specimen thickness (approx. 20%, as shown in Figure 4(b)). Similar analyses were conducted for tensile and compressive specimens, and correction factors were computed from the FE results to scale the average surface strain in the gauge (the quantity measured by DIC) to the average through-thickness gauge strain, as described by Taher, et al. [25]. This methodology has been shown to compensate for errors associated with non-uniform strain distributions arising from the specimen geometry [30]. Specimen dimensions that are not sufficiently large compared to the cell size are another potential source of experimental error in evaluating the elastic moduli of foams, but the specimens in this work are sufficiently large to avoid this effect according to Tekog̃lu et al. [31] and given the cell sizes presented in Table 2.

### **3. Results and Discussion**

#### *3.1 Mechanical Characterization of Pure PU Foams*

Representative tensile, compressive, and shear stress-strain curves for pure PU foam are shown in Figure 5 ( $\rho_f = 128.0 \text{ kg-m}^{-3}$ ). The tensile and compressive moduli in the rise direction of the foam are higher than those in the transverse direction, indicating orthotropic material properties due to an elongated cell shape in the rise direction. The moduli are plotted as a function of density for all pure PU foams in Figure 6, and power law curves in the form of Equation (3) are fitted to the experimental data.

#### *3.2 Mechanical Characterization of Composite PU Foams*

The results of tensile and shear testing of glass-fiber and nanocomposite foams are plotted as a function of density in Figure 7 along with the trend lines for pure PU foams. Nanocomposite foams were also tested in compression and exhibited moduli similar to those in tension. The elastic moduli of the composite foams vary considerably from that of the lab-produced pure PU foam ( $\rho_f = 144.5 \text{ kg-m}^{-3}$ ), but the power law trend for pure PU foams in Figure 7 indicates that much of this variation can be attributed to changes in the density of the composite foams.

The modulus data for composite foams is normalized to the trends with density for pure PU foams and plotted as a function of filler content in Figure 8. The normalized moduli would all equal one if the changes in stiffness of the composite foams were solely attributable to changes in density. Figure 8(a) and (b) highlights the tendency for  $E_1$  to increase and for  $E_2$  to decrease in nanocomposite foams compared with the pure PU foam trend. Glass-fiber composite foams exhibit a less-pronounced increase in  $E_1$  and decrease in  $E_2$  up to a fiber content of 11 wt%, beyond which the normalized moduli tend to all increase by approximately the same amount.

### 3.3 Mechanical and Cell Shape Anisotropy

Considered separately, the moduli of composite foams suggest varying degrees of mechanical reinforcement: the rise-direction tensile modulus implies a 4–26% increase, while the transverse tensile modulus implies as much as a 40% decrease. The changes in the degree of mechanical anisotropy ( $E_1/E_2$ ) corresponding to these divergent trends in the tensile moduli indicate that changes in the cell shape may account for some or all of these mechanical deviations from the pure PU trend.

The cellular microstructure of the lab-produced pure PU ( $\rho_f = 144.5 \text{ kg-m}^{-3}$ ) and composite foams was investigated using scanning electron microscopy. The average cell sizes were measured both in the foam rise and transverse directions according to ASTM standard 3576 [32], and are presented in Table 2. The values of shape anisotropy ratio plotted in Figure 9 were calculated as the ratio of these average dimensions. The cell shape anisotropy was also calculated using the ratio of the Young's moduli ( $E_1/E_2$ ) and Equations (4) or (5) from the rectangular and Kelvin unit-cell material models, respectively. The Kelvin-cell model (Equation (5)) has the additional geometry parameter,  $Q$ , which was used to fit the predicted value of  $R$  to the observed value for the pure PU foam. Estimating the solid PU density ( $\rho_s$ ) to be  $1200 \text{ kg-m}^{-3}$  [1,33], a value of  $Q = 0.5755$  was empirically determined to result in the same value of  $R$  that was measured for the pure PU foam. These values of  $Q$  and  $\rho_s$  that were determined for the pure PU foam were

also used to calculate  $R$  for composite foams and resulted in reasonable agreement between the predicted and observed values, as shown in Figure 9, in which both the measured and the predicted values of shape anisotropy are plotted as a function of filler type and filler content. The values of shape anisotropy measured for pure PU ( $R_{\text{measured}}$ ), and predicted for pure PU using the two cellular models ( $R_{\text{rectangular}}$  and  $R_{\text{Kelvin}}$ ) are designated with horizontal lines for comparison with composite foams. The predicted shape anisotropy ratios resulting from the two different cellular models in Figure 9 exhibit similar trends with filler content, but the Kelvin-cell model values are shifted up by an approximately constant amount of 0.4 from the rectangular-cell model values and are in better agreement with the measured values, which can be attributed to the additional parameter  $Q$  in the Kelvin model. The cell shape for glass-fiber composites is only slightly changed from that of the pure PU foam (within 8%), but  $R$  increases significantly for nanocomposite foams (up to 33%). This larger effect of nano-fillers on the cell shape is consistent with the greater influence of nano-particles on bubble nucleation reported in the literature [19].

### 3.4 Degree of Mechanical Reinforcement

The degree of stiffness reinforcement in composite foams was evaluated as the relative difference between the elastic moduli of composite foams, and the predicted moduli of a hypothetical pure PU foam with the same density and cell shape as the composite foam of interest. This measure of foam reinforcement was calculated by rearranging Equation (3) into the following form:

$$E_f = \left[ \frac{CE_s}{(\rho_s)^n} \right] (\rho_f)^n f(R). \quad (6)$$

The ratio of Equation (6) written for a composite foam (with terms subscripted ‘comp’) and for a pure polymer foam (terms subscripted ‘pure’) yields the expression



$$\frac{(E_f)_{\text{comp}}}{(E_f)_{\text{pure}}} = \left[ \frac{(E_s / (\rho_s)^n)_{\text{comp}}}{(E_s / (\rho_s)^n)_{\text{pure}}} \right] \left( \frac{(\rho_f)_{\text{comp}}}{(\rho_f)_{\text{pure}}} \right)^n \frac{f(R_{\text{comp}})}{f(R_{\text{pure}})}, \quad (7)$$

which may be rearranged into:

$$(E_f)_{\text{comp}} = \frac{(E_f)_{\text{pure}}}{((\rho_f)_{\text{pure}})^n} ((\rho_f)_{\text{comp}})^n \frac{f(R_{\text{comp}})}{f(R_{\text{pure}})} \left[ \frac{(E_s / (\rho_s)^n)_{\text{comp}}}{(E_s / (\rho_s)^n)_{\text{pure}}} \right]. \quad (8)$$

The constant terms and exponents in the equations for the power-law curves in Figure 6(a) were

substituted for the term  $\frac{(E_f)_{\text{pure}}}{((\rho_f)_{\text{pure}})^n}$  and the exponent  $n$ , respectively, and the term

$\left[ \frac{(E_s / (\rho_s)^n)_{\text{comp}}}{(E_s / (\rho_s)^n)_{\text{pure}}} \right]$  was defined as  $\Gamma$ , the degree of foam reinforcement, to yield:

$$(E_1)_{\text{comp}} = 4.495 \times 10^{-2} ((\rho_f)_{\text{comp}})^{1.556} \left[ \frac{f(R_{\text{comp}})}{f(R_{\text{pure}})} \right] \Gamma, \quad (9)$$

$$(E_2)_{\text{comp}} = 1.831 \times 10^{-2} ((\rho_f)_{\text{comp}})^{1.634} \left[ \frac{f(R_{\text{comp}})}{f(R_{\text{pure}})} \right] \Gamma, \quad (10)$$

and

$$(G_{12})_{\text{comp}} = 3.509 \times 10^{-3} ((\rho_f)_{\text{comp}})^{1.810} \left[ \frac{f(R_{\text{comp}})}{f(R_{\text{pure}})} \right] \Gamma. \quad (11)$$

The reinforcement term,  $\Gamma$ , is the ratio of solid stiffness of the composite and pure materials, each normalized by the corresponding solid density raised to the power  $n$ , and accounts for the relative difference between the properties of a composite foam and those of a pure foam with the same density and cell shape. This definition of foam reinforcement requires that the stiffness of the composite material  $((E_s)_{\text{comp}})$  increase relative to its density by at least as much as does the pure foam (i.e. according to a power law with exponent  $n$ ) in order to achieve positive reinforcement ( $\Gamma > 1$ ). This is an appropriate measure of reinforcement for cellular materials because an increase in solid stiffness ( $E_s$ ) that is equal to the  $n$ -power law trend with solid density ( $\rho_s$ ) could be realized by simply reducing the void content of the pure material, and so is not considered reinforcement of the foam.  $\Gamma$  is assumed to be independent of the material

direction in Equations (9-10) because the good agreement between the measured and the predicted shape anisotropy (using the Kelvin model) of composite foams implies that the mechanical anisotropy can be wholly attributed to cell-shape effects. If cellular models had been unable to accurately predict  $R$  for composite foams, then multiple direction-dependent  $\Gamma$  terms could be used in Equations (9-11) to account for factors leading to anisotropy of the solid composite ( $(E_s)_{\text{comp}}$ ), e.g. preferential fiber orientation.

The functions  $f(R)$  in Equations (9–11) were taken from Table 1 for the rectangular-cell model and from the literature for the Kelvin-cell model<sup>4</sup> [7,8], and the calculated values of shape anisotropy from the corresponding cellular model (presented in Figure 9) were used. The reinforcement term,  $\Gamma$ , was determined by minimizing the squared-error between the measured moduli and the moduli predicted using Equations (9–11) for each composite foam, and is plotted for glass-fiber and nanocomposite foams in Figure 10. The normalized moduli calculated using the best-fit values of  $\Gamma$  are shown along with the measured values in Figure 8. The predicted values are in good agreement with the measured moduli for glass-fiber composite foams regardless of the cellular model employed (predicted values are mostly within one standard deviation of the measured value). However, the rectangular cellular model cannot simultaneously predict the in-plane moduli accurately for nanocomposite foams. This failure of the rectangular-cell model is shown in Figure 8(a) and (c), in which the predicted values of  $E_I$  are about one standard deviation above and of  $G_{I2}$  are up to 4 standard deviations below the measured values for nanocomposite foams. The Kelvin-cell model predictions, which are also shown in Figure 8, are in good agreement with measured values (all within one standard deviation). This is consistent with the poor predictions of  $R$  resulting from the rectangular-cell model in Figure 9.

---

<sup>4</sup> The terms related to cellular structure ( $R$ ,  $Q$ ) cannot be isolated from the other terms in the expressions for the foam moduli in the Kelvin-cell model. Consequently, the ratio  $f(R_{\text{comp}})/f(R_{\text{pure}})$  had to be computed numerically as  $E_I(R_{\text{comp}}, Q, (\rho_f)_{\text{comp}}, \rho_s) / E_I(R_{\text{pure}}, Q, (\rho_f)_{\text{comp}}, \rho_s)$  for each composite foam. In all cases, a value  $Q = 0.5755$  and  $\rho_s = 1.2 \text{ kg-m}^{-3}$  was used.

The adequacy of the rectangular-cell model for characterizing the glass-fiber foam properties, despite the large difference between the measured and predicted values of  $R$  using this model (Figure 9), is likely due to the relatively small change in cell shape (and consequently the small mechanical impact of cell shape) in these foams.

The degree of foam reinforcement for glass-fibers shown in Figure 10 is similar regardless of the cellular model used. The values of  $\Gamma$  from the two cellular models are most divergent in foams with the largest changes in  $R$  compared to the pure foam (1.0, 3.0, 5.0, 9.0, and 19.0 wt% milled glass fibers), in which cases the values produced using the Kelvin-cell model are recommended by the more accurate predicted values of  $R$  from this model. There is a relatively small degree of foam reinforcement (2.8–10.7% increase) in foams with 1.0–11.0 wt% glass-fibers, which is the same range of filler content over which  $E_1$  increased while  $E_2$  decreased compared with the pure PU foam trend in Figure 8 (a) and (b). The changes in the normalized moduli over this range of filler content are largely attributable to the mechanical effects of cell shape,  $R$ , rather than stiffening of the solid material. Above a glass-fiber content of 11.0wt%,  $E_1$  and  $E_2$  tended to rise together relative to the pure PU trend, leading to more pronounced increases in the degree of foam reinforcement (up to 18.7%).

Nanocomposite foams offer a more extreme example of divergence in the normalized moduli ( $E_1$  and  $E_2$ ) than any of the glass-fiber foams, which may be attributed to the large increases in  $R$  for these foams (Figure 9). With  $\Gamma$  changing by just 2.4 and -2.4%, the modulus changes in 0.25 and 1.0wt% nanocomposite foams can be almost wholly attributed to changes in cellular structure.

The higher relative values of  $E_2$  and  $G_{12}$  for the 0.5wt% nanocomposite foam resulted in the larger increase in the degree of reinforcement of 11.1%.

#### **4. Conclusions**

Composite PU foams with glass-fibers and hybrid nano-particles were fully characterized in the plane parallel to foaming. The moduli of composite foams were normalized to the trends with

density established for pure PU foams. The normalized moduli of composite foams in the foam rise direction increased by 4–26%, but increased less or even decreased by as much as 40% in the transverse direction. These divergent trends were explained by the increased cell shape anisotropy, which was predicted using cellular mechanics models and confirmed microscopically. The mechanical model based on the Kelvin tetrakaidecahedron unit-cell was favored based on its accurate predictions of cell shape for the specific foams in this study, but a simpler rectangular unit-cell model predicted similar trends and may prove sufficiently accurate for different foams. After accounting for the effects of density and cell shape, any remaining mechanical difference in composite foams was attributed to changes in the properties of the solid ( $E_s$ ,  $\rho_s$ ) through a quantity termed foam reinforcement ( $\Gamma$ ), which was shown to depend on both the stiffness and the density of the solid composite. An isotropic  $\Gamma$  was sufficient to accurately predict the measured in-plane moduli of the foams in this study, but directionally-dependent values of  $\Gamma$  could be considered in cases when the composite solid stiffness ( $(E_s)_{\text{comp}}$ ) is dependent on the material direction, as may be the case for aligned fiber-reinforced foams.

The comparison of reinforced polymer foams with the corresponding pure foam at the same foam density by establishing power-law trends for the pure foams allows a fair comparison between materials with the same density. It should be noted that normalization of the foam modulus to foam density,  $E_f/\rho_f$ , does not necessarily provide for the same comparison between foams of unequal densities. The determination of cell shape contributions to mechanical anisotropy is important for understanding the causes of property enhancement in a given material direction (and the potential trade-offs in other directions), and is relevant for applications with anticipated loads in multiple material directions. This is the case for sandwich panel core materials, which typically experience multi-axial loading conditions in service. In conjunction with composite models to predict the composite solid stiffness ( $(E_s)_{\text{comp}}$ ) and density ( $(\rho_s)_{\text{comp}}$ ),

the definition of foam reinforcement,  $\Gamma$ , provides a tool for predicting the efficacy of reinforcing additives for foams in view of the potential tradeoff between stiffness and added weight.

## Acknowledgments

This work was conducted and financially supported through EU FP7-NMP-2007-2.1-1 large scale integrated project “NanCore”, Grant Agreement No. 214148, and the Department of Mechanical and Manufacturing Engineering, Aalborg University, Denmark. The authors gratefully acknowledge Thomas Sørensen Quaade for his technical assistance, especially with electron microscopy.

- 
- [1] Gibson LJ, Ashby MF. Cellular Solids Structure and Properties. Pergamon Press, Oxford (1988).
  - [2] Roberts AP, Garboczi EJ. Elastic moduli of model random three-dimensional closed-cell cellular solids. *Acta Mater* 2001;49:189–197.
  - [3] Roberts AP, Garboczi EJ. Elastic properties of model random three-dimensional open-cell solids. *J Mech Phys Solids* 2002;50:33–55.
  - [4] Istrate OM, Chen B. Relative modulus-relative density relationships in low density polymer-clay nanocomposite foams. *Soft Matter* 2011;7:1840–1848.
  - [5] Huber AT, Gibson LJ. Anisotropy of polymer foams. *J Mater Sci* 1988;23:3031–3040.
  - [6] Thomson, W. (Lord Kelvin). On the division of space with minimum partitional area. *Phil Mag* 1887;24:503–514.
  - [7] Sullivan RM, Ghosn LJ, Lerch BA. A general tetrakaidecahedron model for open-celled foams. *Int J Solid Struct* 2008;45:1754–1765.
  - [8] Sullivan RM, Ghosn LJ. Shear moduli for non-isotropic, open cell foams using a general elongated Kelvin foam model. *Int J Eng Sci* 2009;47:990–1001.
  - [9] Cotgreave TC, Shortall JB. The mechanism of reinforcement of polyurethane foam by high-modulus chopped fibres. *J Mater Sci* 1977;12:708.
  - [10] Shen H, Nutt S. Mechanical characterization of short fiber reinforced phenolic foam. *Composites, Part A* 2003;34:899–906.
  - [11] Desai A, Auad ML, Shen H, Nutt SR. Mechanical behavior of hybrid composite phenolic foam. *J Cell Plast* 2008;44:15–36.
  - [12] Alonso MV, Auad ML, Nutt S. Short-fiber-reinforced epoxy foams. *Composites, Part A* 2006;37:1952–1960.
  - [13] Neagu RC, Cuénoud M, Berthold F, Bourban P-E, Gamstedt K, Lindström M, Månson J-AE. The potential of wood fibers as reinforcement in cellular biopolymers. *J Cell Plast* 2012;48:71–103.
  - [14] Goods SH, Neuschwanger CL, Whinnery LL, Nix WD. Mechanical properties of a particle-strengthened polyurethane foam. *J Appl Polym Sci* 1999;74:2724–2736.
  - [15] Barma P, Rhodes MB, Salovey R. Mechanical properties of particulate-filled polyurethane foams. *J App Phys* 1978;49:4985–
  - [16] Saint-Michel F, Chazeau L, Cavaillé J-Y. Mechanical properties of high density polyurethane foams: II Effect of the filler size. *Comp Sci Tech* 2006;2709–2718.
  - [17] Yin B, Li Z-M, Quan H, Yang M-B, Zhou Q-M, Tian C-R, Wang J-H. Morphology and mechanical properties of nylon-1010-filled rigid polyurethane foams. *J Cell Plast* 2004;36:333–349.
  - [18] Sorrentino L, Aurilia M, Forte G, Iannace S. Anisotropic mechanical behavior of magnetically oriented iron particle reinforced foams. *J Appl Polym Sci* 2011;119:1239–1247.
  - [19] Lee LJ, Zeng C, Cao X, Han X, Shen J, Xu G. Polymer nanocomposite foams. *Comp Sci Tech* 2005;65:2344–2363.
  - [20] Zhang L, Yilmaz ED, Schjødt-Thomsen J, Rauhe JC, Pyrz R. MWNT reinforced polyurethane foam: Processing, characterization and modelling of mechanical properties. *Comp Sci Tech* 2011;71:877–884.
  - [21] Yan D, Xu L, Chen C, Tang J, Ji X, Li Z. Enhanced mechanical and thermal properties of rigid polyurethane foam composites containing graphene nanosheets and carbon nanotubes. *Polym Int* 2012;61:1107–1114.
  - [21] Lee LJ, Zeng C, Cao X, Han X, Shen J, Xu G. Polymer nanocomposite foams. *Comp Sci Tech* 2005;65:2344–2363.
  - [22] Istrate OM, Chen B. Relative modulus–relative density relationships in low density polymer–clay nanocomposite foams. *Soft Matter* 2011;7:1840–1848.
  - [23] Schjødt-Thomsen J, Pyrz R. Effective properties of cellular materials. *Polym Eng Sci* 2001;41:752–757.

- 
- [24] Verdejo R, Bernal MM, Romasanta LJ, Tapiador FJ, Lopez-Manchado MA. Reactive nanocomposite foams. *Cell Polym* 2011;30:45–61.
- [25] Taher ST, Thomsen OT, Dulieu-Barton JM, Zhang S. Determination of mechanical properties of PVC foam using a modified Arcan fixture. *Composites, Part A* 2012;43:1698–1708.
- [26] Madaleno L, Pyrz R, Jensen LR, Pinto JJC, Lopes AB, Dolomanova V, Schjødt-Thomsen J, Rauhe JC. Synthesis of clay-carbon nanotube hybrids: Growth of carbon nanotubes in different types of iron modified montmorillonite. *Comp Sci Tech* 2012;72:377–381.
- [27] Madaleno L, Pyrz R, Crosky A, Jensen LR, Rauhe JC, Dolomanova V, Viegas de Barros Timmons AMM, Pinto JCC, Norman J. Processing and characterization of polyurethane nanocomposite foam reinforced with montmorillonite–carbon nanotube hybrids. *Composites, Part A* 2013;44:1–7.
- [28] Peters WH, Ranson WF. Digital imaging techniques in experimental stress analysis. *Opt Eng* 1982;21:427–431.
- [29] Chu TC, Ranson WF, Sutton MA. Applications of digital-image-correlation techniques to experimental mechanics. *Exp Mech* 1985;25:232–244.
- [30] Zhang S, Dulieu-Barton J, Freuhmann RK, Thomsen OTT. A methodology for obtaining material properties of polymeric foam at elevated temperatures. *Exp Mech* 2012;52:3–15.
- [31] Tekog̃lu C, Gibson LJ, Pardoen T, Onck PR. Size effects in foams: Experiments and modeling. *Prog Mater Sci* (2011) 56:109–138.
- [32] ASTM 3576 – 04. Standard Test Method for Cell Size of Rigid Cellular Plastics. ASTM International, 100 Barr Harbor Drive, PO Box C700, West Conshohocken, PA 19428-2959, United States.
- [33] Roff, W. F.; Scott, J. R. *Fibres, Films, Plastics and Rubbers—A Handbook of Common Polymers*, Butterworths:London, UK, 1971; p. 445.

Table 1. The functions  $f(R)$  from Equation (3) for the elastic moduli in each material direction, based on a rectangular unit cell.

Property	$f(R)$
$E_1$	$R$
$E_2, E_3$	$\frac{1}{2R} \left[ 1 + \left( \frac{1}{R} \right)^3 \right]$
$G_{12}, G_{13}$	$\frac{2}{R(R+1)}$
$G_{23}$	$\frac{1}{R}$

Table 2. Average cell dimensions measured in pure and nanocomposite PU foams.

Foam	$h$ [ $\mu\text{m}$ ]	$l$ [ $\mu\text{m}$ ]
Pure PU (lab)	389	250
0.25 wt% Nanocomposite	317	182
0.5 wt% Nanocomposite	357	214
1.0 wt% Nanocomposite	340	197
1.0 wt% Glass-fiber	387	249
3.0 wt% Glass-fiber	372	231
5.0 wt% Glass-fiber	458	268
7.0 wt% Glass-fiber	370	227
9.0 wt% Glass-fiber	346	230
11.0 wt% Glass-fiber	360	204
13.0 wt% Glass-fiber	297	205
15.0 wt% Glass-fiber	368	223
17.0 wt% Glass-fiber	386	231
19.0 wt% Glass-fiber	349	215

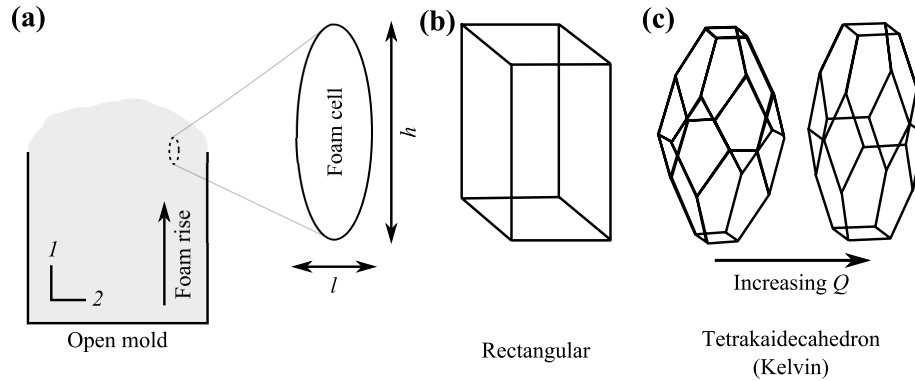


Figure 1. (a) Schematic of polyurethane foaming process with material coordinate system specified, and inset showing a typical elongated cell geometry with dimensions. Cell shape geometries for (b) rectangular, and (c) Kelvin cellular mechanical models (Reproduced and adapted from [8] with permission from Elsevier).

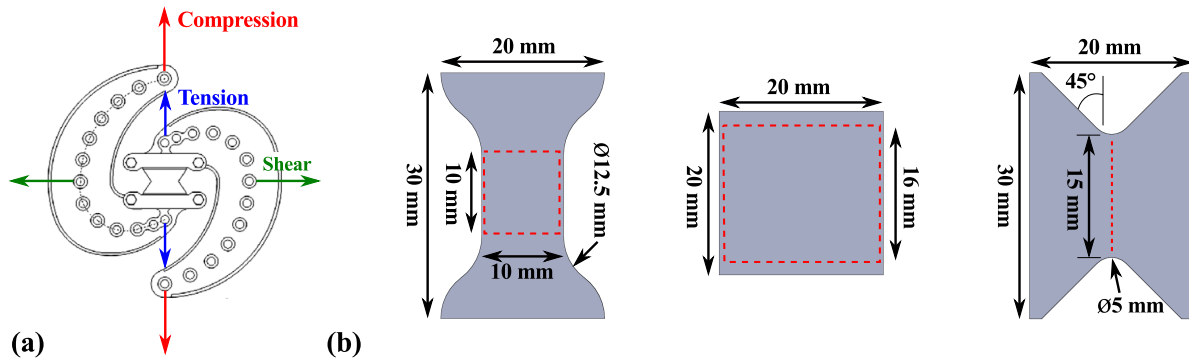


Figure 2. (a) Schematic of modified Arcan fixture, with tensile, compressive, and shear loading configurations specified (Reproduced and adapted from [25] with permission from Elsevier). (b) Specimen geometries for tension, compression, and shear loading configurations (all specimen thicknesses 15 mm). Gauge area/line indicated by dashed red lines.



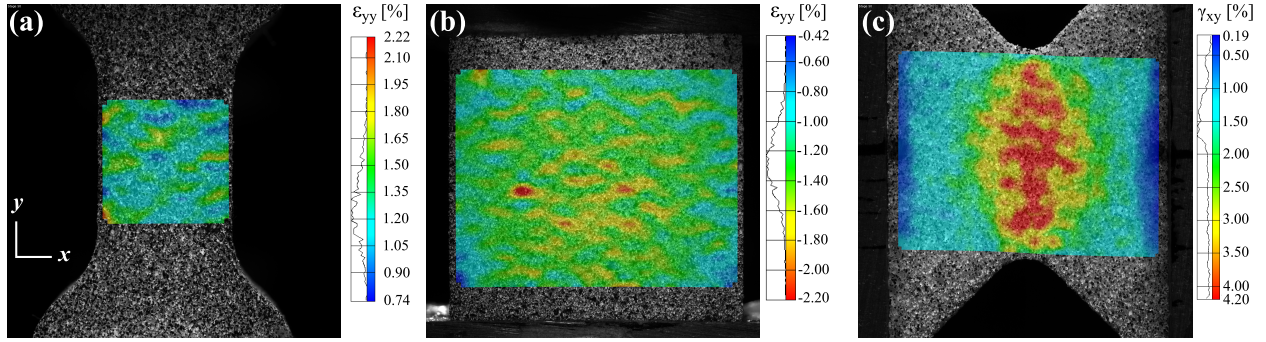


Figure 3. Representative strain fields measured using DIC on a (a) tensile specimen (normal strain in  $y$ -direction shown), (b) compression specimen (normal strain in  $y$ -direction shown), and (c) shear specimen (engineering shear strain in  $x$ - $y$  plane shown). Loading was applied in the  $y$ -direction.

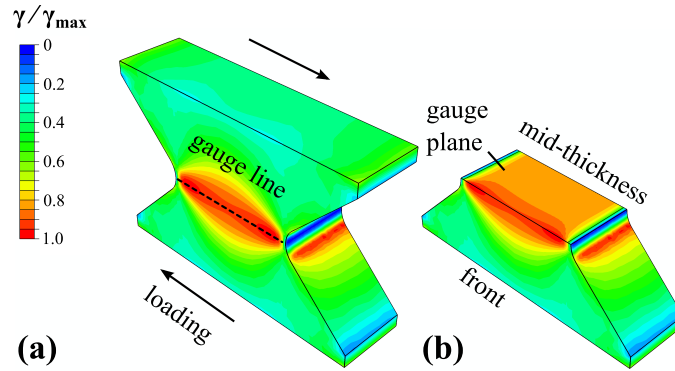


Figure 4. Simulated shear strain distribution in a half-model of a shear specimen (symmetric about the mid-thickness) loaded in the elastic range (a) on the front/back surface, and (b) through the thickness on the plane of the gauge line (cut-away view).

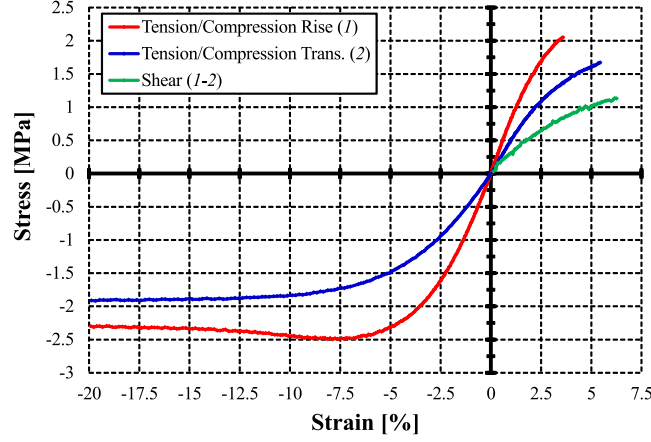


Figure 5. Typical stress-strain curves for pure PU foam ( $\rho_f = 128.0 \text{ kg}\cdot\text{m}^{-3}$ ) loaded in tension and compression in the rise and transverse directions, and shear in the plane of foaming.

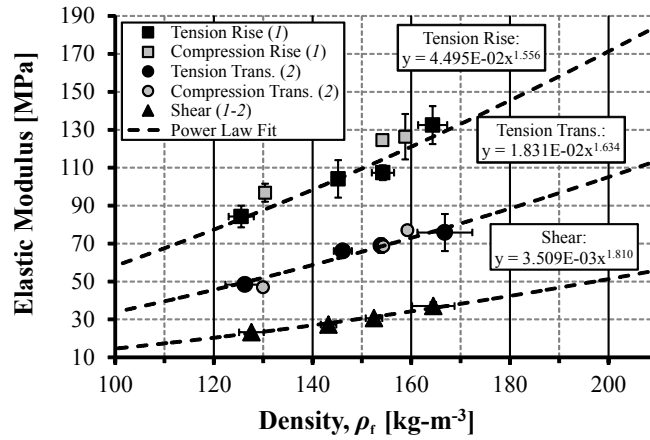


Figure 6. In-plane elastic moduli of pure PU foams at different densities in tension, compression, and shear with power law curves plotted as dashed lines. Each data point represents the average obtained from 5 specimens (except compression, for which 2 specimens were tested) and error bars bound one standard deviation.

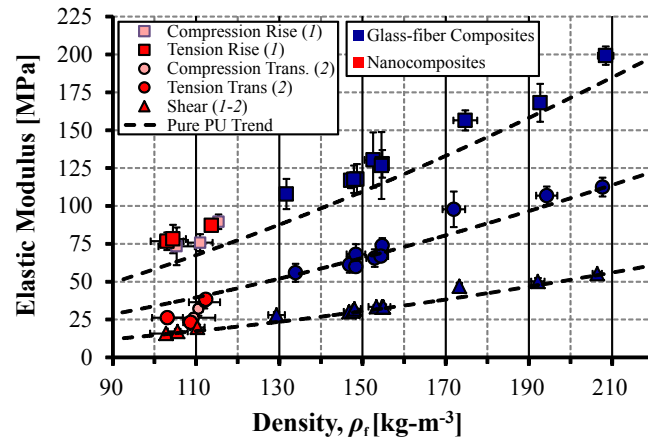


Figure 7. In-plane elastic moduli of glass-fiber (■) and nanocomposite foams (■) in tension, compression, and shear as a function of density. Each data point represents the average obtained from 4 specimens and error bars bound one standard deviation.

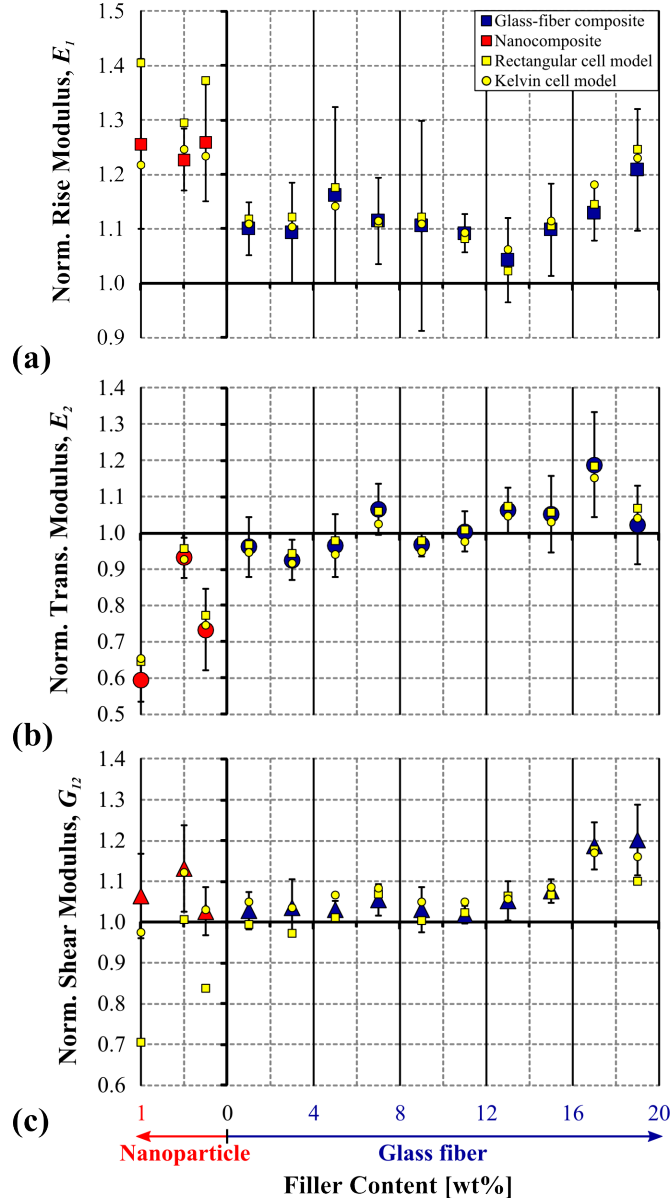


Figure 8. Tensile moduli in the (a) rise and (b) transverse directions, and (c) shear moduli of nanocomposite (■) and glass-fiber foams (■) normalized to the pure PU trend as a function of filler content, with predicted values from Equations (9–11) using the best-fitting  $\Gamma$  from both rectangular and Kelvin unit-cell models.

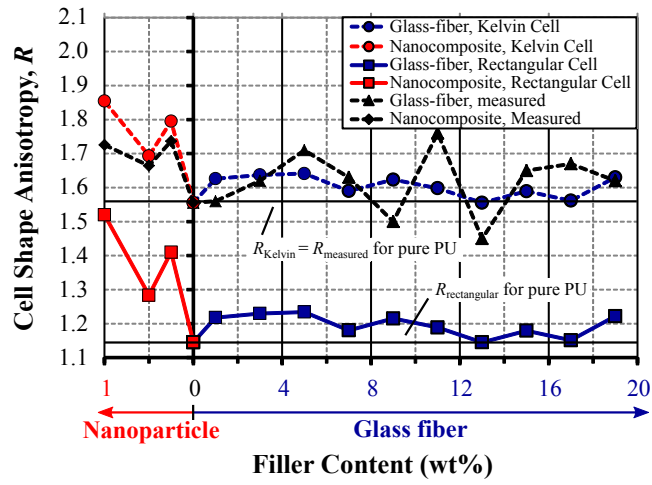


Figure 9. Microscopically measured and predicted (using both rectangular or Kelvin cell models) cell shape anisotropy of pure PU (0 wt% filler) and composite foams as a function of filler content.

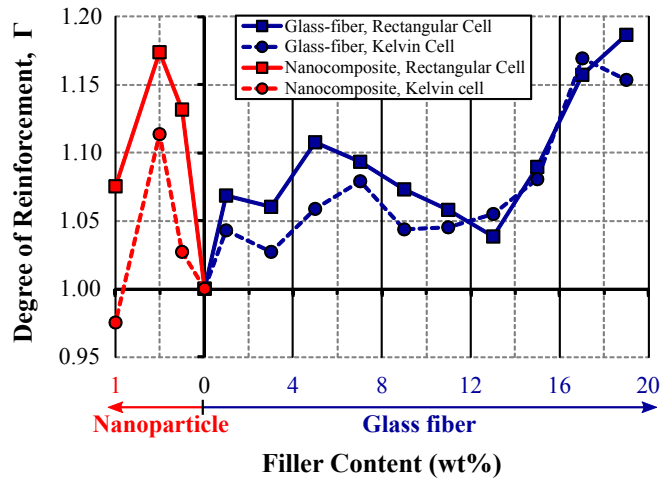


Figure 10. Degree of reinforcement calculated for composite foams using rectangular and Kelvin cellular material models.